Squeezing particle-stabilized emulsions into biliquid foams – supplementary information

Louison Maurice[a,b], Ryan A. Maguire[a], Andrew B. Schofield[a],
Michael E. Cates[a], Paul S. Clegg[a] and Job H. J. Thijssen[*a]

June 19, 2013

[a]*SUPA, School of Physics & Astronomy, The University of Edinburgh, Edinburgh, EH9 3JZ, United Kingdom. E-mail: j.h.j.thijssen@ed.ac.uk*
[b]*Current address: École Normale Supérieure de Lyon, Université Claude Bernard Lyon I, Lyon, France*

1 Quick guide

2 Sample information

See Table 1 for an overview of the composition of emulsion samples used and Table 2 for an overview of colloidal particles used.

3 Emulsion characterization

3.1 Interfacial Tension

The interfacial tension between the oil and aqueous phases of the transparent system was measured using the pendant-drop technique. Oil (DC550 : CHB = 80.5 : 19.5 w/w) and aqueous (60 wt-% sodium iodide) phases were prepared and allowed to homogenize separately on a rollerbank for at least 12 h. Note that we used 60 wt-% sodium iodide for these measurements, as the phases are so well matched at 65 wt-% that the droplet profile cannot be fitted. The less dense oil phase was loaded into a cubic glass cuvette ($20 \times 20 \times 20$ mm^3), which was sealed with parafilm to inhibit CHB evaporation, while a glass syringe was filled with the denser aqueous phase. The outer diameter of the needle was measured to be 1.840 mm (vernier caliper, Mitutoyo). A spirit level was used to ensure the tensiometer (Krüss EasyDrop, model FM40Mk2) was properly aligned, while a thermocouple (Type K) was employed to monitor the temperature near the cuvette. Due to the relatively high density of the aqueous phase, droplets larger than ~ 10 μL eventually fell off the needle. Hence, measurements were performed on ~ 6.4 μL and ~ 8.9 μL droplets, which were delivered at a set rate of 100 μL/min using a software-controlled dosing unit. Pendant drops were monitored up to 150 minutes, during which digital photographs were recorded from the side. Volume and interfacial-tension values were extracted by fitting the Young-Laplace equation to the recorded droplet profiles. These values initially decreased, but leveled off after approximately 60 min. To double-check our measurements, we measured the surface tension of a pendant water droplet in air at 23 °C ($\gamma = 73.5$ mN/m), which is only 1.5% higher than literature values ($\gamma \approx 72.4$ mN/m).[3]

Table 1: Sample compositions: φ volume fraction of colloidal particles in total emulsion volume, W/O v/v water/oil volume ratio, $R = R_{32}$ Sauter mean droplet radius, PD droplet polydispersity, N number of droplets measured for sizing, Δ sample extracted for microscopy and o(t) opaque(transparent) samples.

Sample	Volume / mL	Particle	φ (%)	W/O v/v	R / μm	PD (%)	N	Δ(sample)
R28o	12.1	PMMA063	4.3	40/60	28.0	37	293	0.478 g
R38o	12.1	PMMA063	3.0	40/60	38.1	42	347	0.411 g
R43o	12.1	PMMA063	2.2	40/60	42.6	32	239	0.423 g
R58o	12.1	PMMA063	1.8	40/60	58.3	25	325	0.459 g
R31o	12.0	PMMA139-PLMA	10	40/60	31.0	–	100	$\sim$ 0.13 mL
R39o	12.0	PMMA110	7.8	40/60	39.0	–	100	$\sim$ 0.13 mL
R34o	12.0	PMMA063-PDV	4.5	40/60	33.9	–	100	$\sim$ 0.13 mL
R33o	12.0	PMMA058	4.1	40/60	32.8	–	100	$\sim$ 0.13 mL
R25t	–	PMMA063	4.0	40/60	24.7	54	254	n/a
R44t	–	PMMA063	2.0	40/60	44.1	23	170	n/a
R67t	–	PMMA063	1.3	40/60	66.6	–	111	n/a
R86t	–	PMMA063	0.9	40/60	85.6	–	94	n/a

Table 2: Particle batches: SLS Static Light Scattering, * bimodal with $r_{\text{TEM}} = 1.30$ and 0.56 μm, NBD 4-chloro-7-nitrobenzo-2-oxa-1,3-diazol, PHSA poly(12-hydroxystearic acid), PDV Gelest PDV-2335[1] and PLMA poly(lauryl methacrylate).[2]

Sample	Radius / μm (SLS)	Polydispersity (%) (SLS)	Fluorescent dye	Stabilizer
PMMA063	0.630	9	NBD	PHSA
PMMA058	0.575	5	NBD	PHSA
PMMA110	1.100	2	NBD	PHSA
PMMA063-PDV	0.625	3.5	Nile Red	PDV
PMMA139-PLMA	1.390*	3	none	PLMA

2

3.2 Droplet sizing

In the case of opaque samples, to measure the Sauter mean or surface average droplet radius $\langle R \rangle = R_{32}$ and polydispersity PD,

$$\langle R \rangle = R_{32} = \frac{\sum_{i=1}^{N} R_i^3}{\sum_{i=1}^{N} R_i^2} \ , \tag{1}$$

$$\text{PD} = \frac{1}{R_{\text{med}}} \frac{\sum_{i=1}^{N} R_i^2 \left| R_i - R_{\text{med}} \right|}{\sum_{i=1}^{N} R_i^2} \ , \tag{2}$$

in which R_{med} is the median radius,[4] a small amount of (similar) emulsion was carefully transferred by pipette from the sample vials to closed or open glass cuvettes (Starna, path length ≥ 1 mm). After dilution with n-dodecane (as and when required), a confocal microscope (see main text) or an Olympus BX50 upright microscope, equipped with a $10\times/0.25$NA objective, was used to take pictures at various positions along the samples. The optical-microscopy images were calibrated using an 80 lines/mm slide. At least 94 droplets were manually sized using the 'Measure & Label' feature in ImageJ (Table 1).[5] In the case of transparent samples, part of the emulsion was carefully transferred by pipette from the sample vials to glass cuvettes and imaged using a confocal microscope prior to centrifugation. Droplet areas were extracted using image analysis and converted to radii for statistical analysis.

3.3 Specific surface area

Assuming that all colloidal particles end up at a liquid-liquid interface, the droplet radius is inversely proportional to the mass of particles added m_p,[4]

$$\frac{1}{\langle R \rangle} = \frac{s_f m_p}{3 V_d} \ , \tag{3}$$

in which s_f is the specific surface area and V_d is the volume of the dispersed phase (water + particles). By fitting a straight line through the origin to the data in Fig. 1, we obtain $s_{f,\text{opaque}} (\text{PMMA063}) = 0.96 \ \text{m}^2 \cdot \text{g}^{-1}$ and $s_{f,\text{transparent}} (\text{PMMA063}) = 1.08 \ \text{m}^2 \cdot \text{g}^{-1}$ (Table 2).

One can also predict s_f theoretically using

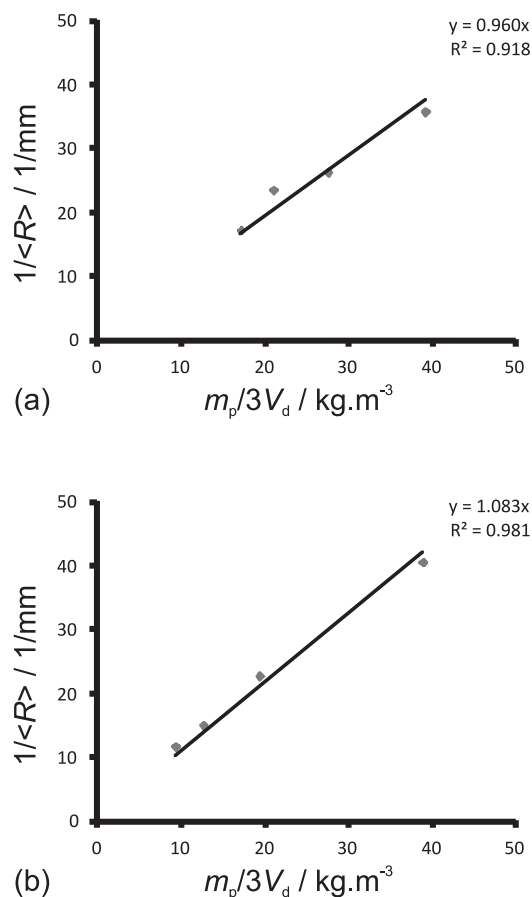$$s_{f,\text{theory}} = \frac{3}{4 C \rho_p r} \ , \tag{4}$$

(a)

(b)

Figure 1: Graphs for determining s_f for PMMA063 by fitting Eq. (3) to the data corresponding to (a) the opaque system (water-dodecane/PMMA) and (b) the transparent system (water(NaI)-DC550CHB/PMMA). Legends: functions used for fit and coefficients of determination (R^2).
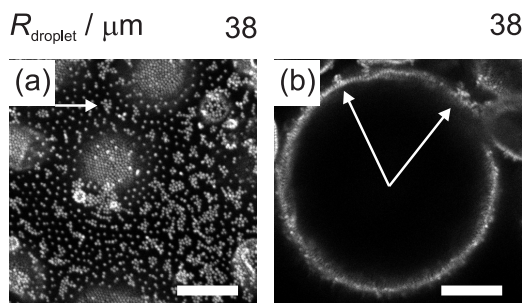
3

R_{droplet} / µm   38   38

Figure 2: Confocal micrographs of an (opaque) water-in-dodecane emulsion, stabilized by 0.630 µm radius PMMA-PHSA particles (white), prior to centrifugation. (a) Close to the cuvette wall (arrow: aggregate in continuous phase) and (b) halfway through the first layer of droplets (arrows: interfacial aggregates). Scale bars 25 µm.
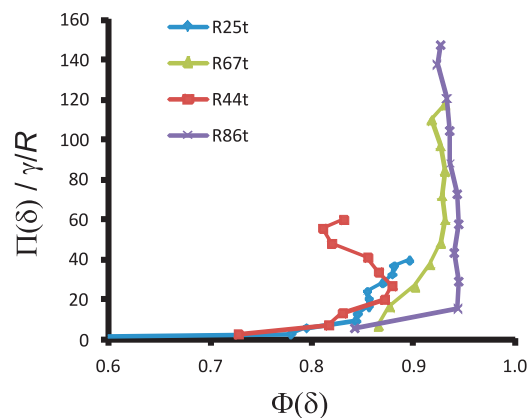

Figure 3: Local osmotic pressure $\Pi(\delta)$ vs local droplet volume fraction $\Phi(\delta)$, as determined via confocal microscopy, for four transparent water-in-oil emulsions stabilized by 0.630 µm radius PMMA-PHSA particles, after centrifugation at $\sim 263g$. Legend: R38t means $R = 38$ µm in transparent sample.

in which ρ_{p} is the mass density of the particles, r their average radius and C the proportion of interfacial area occupied by the particles ($C = \pi/\left(2\sqrt{3}\right)$ for monodisperse particles in a hexagonal lattice).[6] For our system, $s_{\text{f,theory}}$ (PMMA063) $= 1.13$ m$^2 \cdot$ g^{-1}. As $s_{\text{f,opaque}} \lesssim s_{\text{f,theory}}$, we conclude that some particles are not attached to a liquid-liquid interface, because 1) they have been left behind in the continuous phase (even though the supernatant was clear after emulsification) or/and 2) they are trapped in interfacial aggregates (Fig. 2). Note that $s_{\text{f,transparent}} \sim s_{\text{f,theory}}$, implying that the particles were well dispersed in this system, as verified by confocal microscopy.

3.4   Image analysis

In order to extract local dispersed-phase volume fractions $\Phi(\delta)$ from 3D confocal image series, background and dark stacks were acquired in the sample supernatants. Occasionally, different gain settings were used to correct for PMT detector overexposure, for which we linearly corrected during

image analysis. $\Phi(\delta)$ was then extracted as:

$$
\begin{aligned}
\Phi(\delta) &= 1 - \Phi_{\text{oil}}(\delta) \\
&= 1 - \frac{n_{\text{oil,tot}}}{n_{\text{tot,tot}}} \\
&= 1 - \sum_{j=1}^{n_{\text{frames}}} \frac{n_{\text{oil},j}}{n_{\text{tot},j}} \\
&= 1 - \sum_{j=1}^{n_{\text{frames}}} \frac{n_{\text{oil},j}\langle I_{\text{oil}}\rangle_j}{n_{\text{tot},j}\langle I_{\text{oil}}\rangle_j} \\
&= 1 - \sum_{j=1}^{n_{\text{frames}}} \frac{\left(I_{\text{data},j}-I_{\text{dark},j}\right)}{\left(I_{\text{background},j}-I_{\text{dark},j}\right)} \\
&= 1 - \frac{\left(I_{\text{data,tot}}-I_{\text{dark,tot}}\right)}{\left(I_{\text{background,tot}}-I_{\text{dark,tot}}\right)} ,
\end{aligned} \tag{5}
$$

in which $n_{\text{oil,j(tot,j)}}$ is the number of oil(all) pixels in image frame j, n_{frames} is the number of image frames in the confocal stack, $\langle I_{\text{oil}}\rangle_j$ is the average intensity value of an oil pixel in image frame j, $I_{\text{data/background/dark},j}$ is the total intensity value of frame j for the data/background/dark stack and $I_{\text{data/background/dark,tot}}$ is the total intensity value of all frames for the data/background/dark stack. All quantities in the last line of Eq. (5) can easily be obtained from the corresponding stacks in either IDL (RSI v6.4) or ImageJ.[5] Note that we have also determined Φ by counting 'oil' pixels using thresholding, leading to qualitatively similar results, but the thresholding procedure requires several image enhancement steps.

From $\Phi(\delta)$ as determined using Eq. (5), we calculate $\Pi(\delta)$ using

$$\Pi(\delta) = (\rho_{\mathrm{d}} - \rho_{\mathrm{o}})\,\omega^2\delta \int_{d_{\mathrm{c}}-H}^{d_{\mathrm{c}}} \Phi(\delta')\,\mathrm{d}\delta' \; , \quad (6)$$

in which $\rho_{\mathrm{d}}(\rho_{\mathrm{o}})$ is the average density of the particle-laden droplets (continuous oil phase) and ω is the angular frequency of the centrifuge (Fig. 3).[7,8] The integral is evaluated by numerical integration of the data, i.e. we approximate the area under the $(\Phi(\delta),(\delta - (d_{\mathrm{c}} - H)))$-graph as adjacent rectangles centered at the measured values of $(\delta - (d_{\mathrm{c}} - H))$. Instead, one can fit a functional form to the $(\Phi(\delta),(\delta - (d_{\mathrm{c}} - H)))$-graph first and subsequently integrate that function. This leads to similar results, but doesn't work well for sample R44t for example, which is a direct consequence of the fluctuations in the corresponding $(\Phi(\delta),(\delta - (d_{\mathrm{c}} - H)))$-data. These fluctuations are probably due to a relatively low contrast, i.e. data-to-background ratio, in that particular data set.

4 Estimating errors

For opaque samples, errors in the droplet volume fraction Φ and the normalized osmotic pressure $\Pi/(\gamma/R)$ were estimated following Squires.[9] Consider, for example, the error $\sigma_{\Phi(H)}$ in Φ due to the measurement error σ_H in H:

$$\sigma_{\Phi(H)} = \Phi(H + \sigma_H) - \Phi(H) \; . \quad (7)$$

Similar errors in Φ from A, ρ_{p}, the effective thickness of the bottom of the vial H_{b} and the average density of the emulsion sample extracted for microscopy are then combined using:

$$\sigma_{\Phi} = \sqrt{\sigma_{\Phi(H)}^2 + \sigma_{\Phi(A)}^2 + \dots} \; . \quad (8)$$

Similarly, $\sigma_{\Pi/(\gamma/R)}$ is estimated from errors in Φ, H, H_{b}, A, R and a_{c}, while $\sigma_{a_{\mathrm{c}}}$ was estimated from errors in ω, d_{c}, H and H_{b}. Note that contributions of other variables, which were at least $3\times$ smaller than the largest contribution, were considered negligible and therefore ignored.

5 Effect of particle size on equation of state

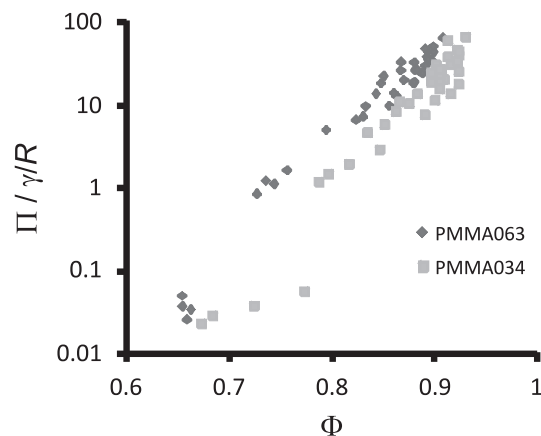See Fig. 4 for the effect of particle size on the equation of state of Pickering-Ramsden emulsions.

Figure 4: Measured osmotic pressure Π vs droplet volume fraction Φ of emulsions stabilized by 0.630 μm or 0.340 μm radius particles (γ: liquid-liquid interfacial tension, R: mean droplet radius, PMMA063: 28 μm $\leq R \leq$ 58 μm and PMMA034: 24 μm $\leq R \leq$ 61 μm). Note that PMMA034 samples were not tapped during initial sedimentation, were re-emulsified prior to each centrifugation and could not be corrected for post-centrifugation recovery (mainly affects graph for moderate Φ).[10]

6 Droplet volume fraction gradient

In the case of opaque PR emulsions, we analyze our data assuming that the droplet volume fraction Φ is constant along the sediment, which is partly justified by Fig. 6(a) in the main text. Alternatively, the data can be analyzed using a method proposed by Tcholakova et al.[11] First, we construct the dependence of the sediment height H on $\ln(a_{\mathrm{c}}/g)$, in which a_{c} is the centrifugal and g the gravitational acceleration. Next, this dependence is interpolated with a continuous empirical function (Fig. 5(a)),

which is then substituted into

$$\Phi_{\text{edge}}(H) = \frac{V_{\text{w}} + V_{\text{p}}}{A} \cdot \frac{1}{H \left(1 + \frac{\text{d} \ln H}{\text{d} \ln (a_{\text{c}}/g)}\right)} \quad . \quad (9)$$

Here, $V_{\text{w}}(V_{\text{p}})$ is the volume of the water (particles) and A is the internal cross-section of the vial (main text Fig. 1). The result of this analysis for R38o is shown in Fig. 5(b), together with the original graph from Fig. 4(b) in the main text. It is clear that both analyses yield qualitatively similar results, though Φ_{edge} is slightly larger than Φ from Eq. (4) in the main text. This is no surprise, as Φ_{edge} is measured at the bottom edge of the sediment, whereas Φ is the average value along the sediment.

7 Emulsion recovery

After centrifugation (stopped at $t = 0$), the time evolution of the samples was monitored at intervals $\Delta t = 5, 10, 15$ or 30 min from $t_{\text{i}} = (8 \pm 3)$ min up to 24 h (240 h in one experiment) using a Labview controlled webcam (Logitech). The change in height ΔH was extracted from the image series in either ImageJ (v1.42q[5]) or IDL (RSI v6.4) by determining the area fraction, α, of pixels above the threshold in a rectangular region-of-interest (ROI) extending from the sediment into the supernatant:[12]

$$\Delta H = \alpha \cdot H_{\text{ROI}} \quad . \quad (10)$$

Using ΔH (averaged over the 3 positions around the vial facing the webcam), H_{final} (the average height of the emulsion sediment as measured using a mounted dial ruler at 8 positions around the vial after the expansion[13]) and a linear extrapolation to account for small differences in webcam starting times, the initial height H can be estimated,

$$H = H (t = 8 \text{ min}) = H_{\text{final}} - \Delta H , \quad (11)$$

Monitoring the post-centrifugation time evolution of our PR emulsions from $t_{\text{i}} = (8 \pm 3)$ min up to 24 h (Fig. 6(a)) allows us to quantify their recovery

$$\xi = \frac{\Delta H}{H_{\text{sed}} - H} , \quad (12)$$

in which H_{sed} is the emulsion-sediment height before centrifugation, ΔH is the recovered height after centrifugation and H is the post-compression
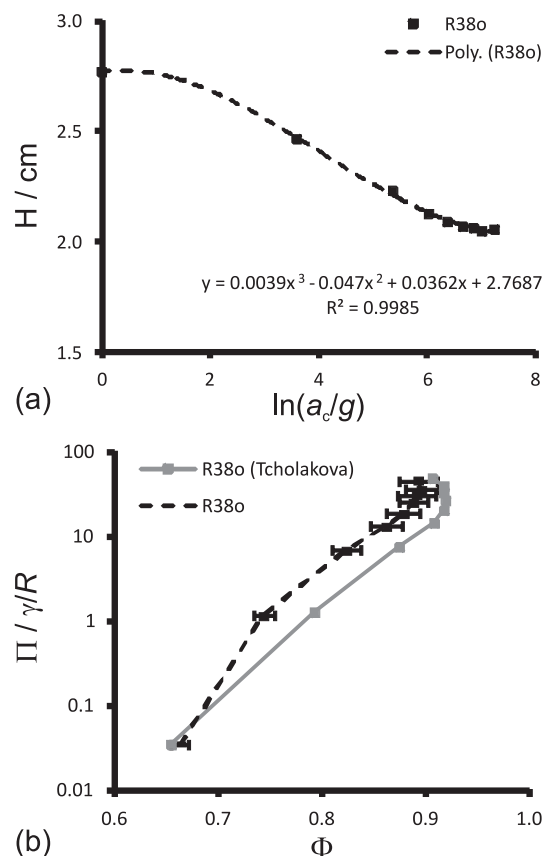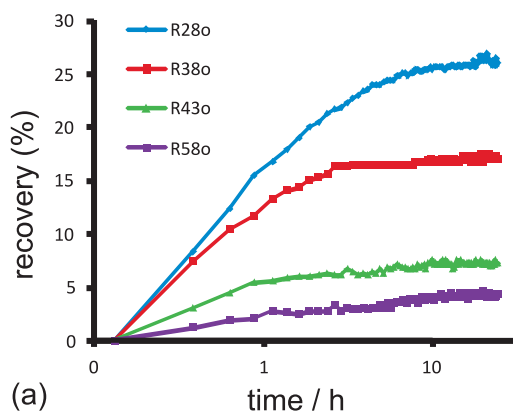

(a)

(b)

Figure 5: (a) Sediment height H vs $\ln(a_{\text{c}}/g)$, in which a_{c} is the centrifugal and g the gravitational acceleration; the solid symbols represent the experimental data, the dashed line is a third-order polynomial fit (see equation in graph and coefficient of determination R^2). (b) Osmotic pressure Π vs droplet volume fraction Φ: the black error bars are the average of Φ along the sediment, whereas the grey symbols correspond to Φ_{edge} at the bottom edge of the sediment (lines are guides to the eye).

6

Figure 7: Recovery (Eq. (12)) of water-in-dodecane emulsions, stabilized by PMMA139-PLMA, PMMA110, PMMA063-GDV and PMMA 058 (Table 2), after centrifugation at 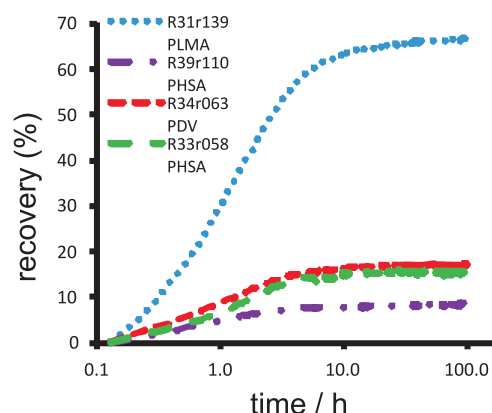$\sim 750g$. R39: mean droplet radius $R = 39$ μm; r110 means particle radius 1.100 μm, etc; lines are guides to the eye.
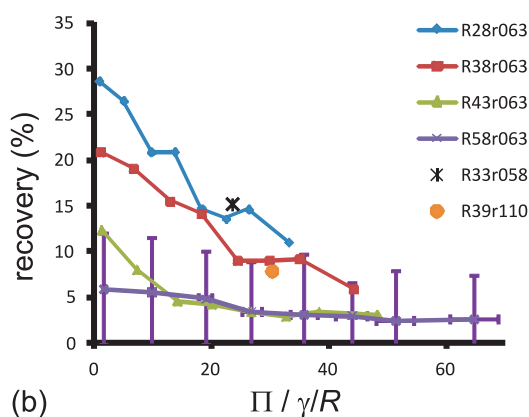
Figure 6: (a) Recovery (Eq. (12)) of water-in-dodecane emulsions, stabilized by 0.630 μm radius PMMA-PHSA particles, after centrifugation at $\sim 194g$. R28o: mean droplet radius $R = 28$ μm in opaque sample. (b) Recovery vs osmotic pressure; only R58 errors plotted for clarity; r063 means particle radius 0.630 μm, etc.

height of the emulsion sediment. From the corresponding graphs in Fig. 6(b), two clear trends emerge. First of all, emulsions with smaller droplets recover more, which is due to their larger Laplace pressure providing a larger restoring force.[7,14,15] Secondly, larger applied osmotic pressures result in less recovery. Intriguingly, changing the steric stabilizer from PHSA or a siloxane copolymer (PDV[1]) to poly(lauryl methacylate) (PLMA[2]) (Table 2), significantly increases the recovery (Fig. 7). This striking result agrees with the finding that PLMA may be a more efficient stabilizer than PHSA, i.e. the area of PMMA stabilized per unit weight of PLMA is somewhat greater.[2]

8   Accounting for particles in interdroplet film

In Sec. 3 of the main text, we defined the interdroplet-film thickness h as the distance between the liquid-liquid interfaces of two neighbouring droplets. Without correction, this would result in part of the colloid volume being counted as continuous rather than dispersed phase. To compen-

7

sate, we subtract from h a thickness h_{p} corresponding to the volume of particles residing in the film but which should be counted as part of the droplet.

To derive an (approximate) expression for h_{p}, we consider an undeformed water droplet coated with particles of radius r and contact angle θ. This droplet contains a volume v_{w} of water, a volume $v_{\text{p}} = n_{\text{ip}} v_{\text{1p}}$ of n_{ip} interfacial particles and a volume v_{o} of oil (trapped between the water, the particles and an imaginary sphere circumscribing the particle-coated droplet). We then construct a volume-equivalent droplet, i.e. a spherical core of volume v_{w}, surrounded by a concentric shell of volume v_{p} and an outer shell of volume v_{o}. For this volume-equivalent droplet, we know that

$$h_{\text{p}} = 2\left(R_{\text{w+p}} - R_{\text{w}}\right) , \tag{13}$$

where R_{w} is the radius of the water core and $R_{\text{w+p}}$ is the outer radius of the particulate shell.

For our experiments, we will assume that

$$R_{\text{w+p}} = R_{32} = R , \tag{14}$$

which is definitely the case for droplet sizing via confocal microscopy and probably not far from the truth for sizing by optical microscopy (Sec. 3.2). Furthermore, due to volume conservation, we can write

$$R_{\text{w}} = R\left(1 - n_{\text{ip}}\left(\frac{r}{R}\right)^3\right)^{1/3} . \tag{15}$$

Assuming a monolayer of closely packed particles on the original droplet and neglecting the curvature of the liquid-liquid interface at the length scale of the particles ($r \ll R$), we can derive that

$$n_{\text{ip}} \approx \frac{12\left(R/r\right)^2}{(3/\kappa) + 8 \cdot c\left(\pi - \theta\right) \cdot (r/R)} . \tag{16}$$

Here, $\kappa \approx \left(\pi\sqrt{3}/6\right)$ is the maximum 2D packing fraction of spheres and

$$c\left(\pi - \theta\right) = \frac{1}{2} + \frac{3}{4}\cos\left(\pi - \theta\right) - \frac{1}{4}\cos^3\left(\pi - \theta\right), \tag{17}$$

which stems from the particles on the original droplet being partly submerged in the water phase.

9   Sliding contact line

In Sec. 3 of the main text, we introduce an effective repulsion per unit area $v\left(h\right) = \alpha\gamma$ between the

droplets to explain the observed Π-enhancement. Assuming a fixed contact line, we argued that $\alpha \sim 1$, as compression requires deformation of the liquid-liquid interface between the particles on one droplet, the energy penalty for which should be of the order of the interfacial tension γ. We also mentioned that assuming a constant contact angle should lead to the contact line sliding across the particle, resulting in two additional contributions to the interaction energy, one from the change in wetted particle surface by the two liquids and one from the change in liquid-liquid contact area.

Straightforward (but tedious) geometric considerations show that the change in free energy upon compression due to a sliding contact line can be expressed as:

$$
\begin{aligned}
\Delta G_{\text{slide}} = \ & 2\pi r^2 \cos\left(\pi - \theta\right)\left(\gamma_{\text{po}} - \gamma_{\text{pw}}\right) \\
& - 2\pi r^2 \cos\left(\pi - \theta + \vartheta\right)\left(\gamma_{\text{po}} - \gamma_{\text{pw}}\right) \\
& + \pi r^2 \gamma\left(\sin^2\left(\pi - \theta + \vartheta\right) - \sin^2\left(\theta\right)\right) .
\end{aligned}
\tag{18}
$$

Here, r is the particle radius, θ is the particle-liquid-liquid contact angle, ϑ is the angle between the deformed and undeformed liquid-liquid interface at the contact line, $\gamma_{\text{po}}(\gamma_{\text{pw}})$ is the particle-oil (water) interfacial tension and γ is the water-oil interfacial tension. If the contact angle remains constant during compression, it obeys Young's equation

$$\gamma_{\text{po}} - \gamma_{\text{pw}} = \gamma \cos\left(\theta\right) . \tag{19}$$

Combining Eqs. (18) and (19) results in

$$
\begin{aligned}
\Delta G_{\text{slide}} = \ & \pi r^2 \gamma \left(2\cos^2\left(\pi - \theta\right)\right. \\
& - 2\cos\left(\pi - \theta\right)\cos\left(\pi - \theta + \vartheta\right) \\
& \left. + \sin^2\left(\pi - \theta + \vartheta\right) - \sin^2\left(\theta\right)\right) .
\end{aligned}
\tag{20}
$$

Note that we write $\left(\pi - \theta\right)$ as the contact angle is measured through water whereas the liquid in the interdroplet film is oil. Eq. (20) confirms that $\Delta G_{\text{slide}} \propto \gamma$, so we can indeed write $v\left(h\right) = \alpha\gamma$ regardless of whether the contact line or the contact angle remains constant upon compression.

In addition, we can write the distance that the contact line slides along the direction perpendicular to the undeformed liquid-liquid interface as

$$\Delta z_{\text{slide}} = 2r\sin\left(\pi - \theta + \frac{\vartheta}{2}\right)\sin\left(\frac{\vartheta}{2}\right) . \tag{21}$$

Sweeping ϑ as a parameter, we can plot ΔG_{slide} vs Δz_{slide} (Fig. 8). Note that even if the contact
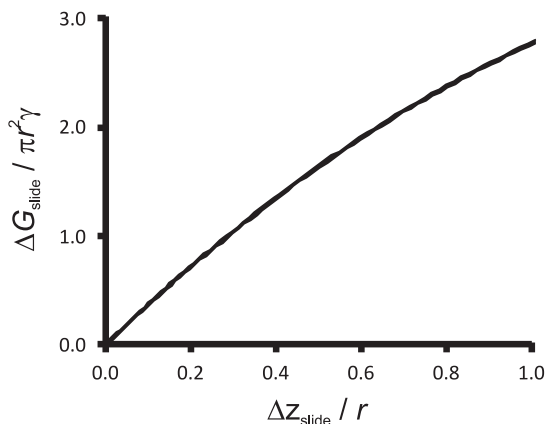
Figure 8: Change in free energy $\Delta G_{\mathrm{slide}}$ upon compression due to the particle-liquid-liquid contact line sliding over a distance $\Delta z_{\mathrm{slide}}$ along the direction perpendicular to the undeformed liquid-liquid interface at constant contact angle (particle radius r and liquid-liquid interfacial tension γ).

line only slides by a quarter of the particle radius, $\Delta G_{\mathrm{slide}}/\left(\pi r^2\gamma\right) \sim \alpha \sim 1$, confirming that the contribution of a sliding contact line to $v\left(h\right)$ can indeed be comparable to the contribution from the deformation of the liquid-liquid interface.

10 Interparticle interactions

To estimate the order of magnitude of capillary forces, we consider here the immersion capillary force between two vertical cylinders of radius $r_{\mathrm{c}} = r$ perpendicular to the liquid-liquid interface. Following Ref.[16] we write

$$\begin{aligned} \Delta W_{\mathrm{im}} &\sim & -2\pi\gamma r_{\mathrm{c}}\sin\left(\Psi_{\mathrm{c}}\right)\left(h_{\mathrm{c}} - h_{\infty}\right)\\ &\sim & 10^8\ k_{\mathrm{B}}T_0\ , \end{aligned}\tag{22}$$

where

$$\begin{aligned} \sin\left(\Psi_{\mathrm{c}}\right) &=& \cos\left(180° - \theta\right)\\ h_{\mathrm{c}} &=& r_{\mathrm{c}}\sin\left(\Psi_{\mathrm{c}}\right)\left(\tau_1 + 2\ln\left(\tfrac{1-\mathrm{e}^{-2\tau_1}}{\gamma_{\mathrm{e}}qa}\right)\right)\\ h_{\infty} &=& r_{\mathrm{c}}\sin\left(\Psi_{\mathrm{c}}\right)\ln\left(\tfrac{4}{\gamma_{\mathrm{e}}qr_{\mathrm{c}}(1+\cos\left(\Psi_{\mathrm{c}}\right))}\right), \end{aligned}\tag{23}$$

and

$$\begin{aligned} \tau_1 &=& \ln\left(\tfrac{a}{r_{\mathrm{c}}} + \sqrt{1 + \tfrac{a^2}{r_{\mathrm{c}}^2}}\right)\\ a &=& \sqrt{L^2 - r_{\mathrm{c}}^2}\ . \end{aligned}\tag{24}$$

Note that, for $h_{\infty} = h_{\mathrm{min}} = 3.47r < 4r$ for a close-packed bilayer, the particles are effectively 'immersed' in the interdroplet film. The associated attractive capillary interaction energy of order $10^8\ k_{\mathrm{B}}T_0$ between particles on the same droplet may be large enough to cause an effective repulsion $\pi r^2 v\left(h_{\mathrm{min}}\right) \sim 10^7\ k_{\mathrm{B}}T_0$ between facets across the interdroplet film, ultimately resulting in the observed osmotic-pressure enhancement.

Below, we estimate the magnitude of various other interparticle interactions and demonstrate that they are too small to make a substantial contribution to the observed Π-enhancement. First, we consider Van der Waals forces. Following Ref.[4] we write

$$\begin{aligned} \Delta W_{\mathrm{VdW}} &\sim & \tfrac{2rA}{12(L-r)}\\ &=& \tfrac{A}{6((L/r)-1)}\\ &\approx & 10^1\ k_{\mathrm{B}}T_0\\ &\ll & 10^7\ k_{\mathrm{B}}T_0\ , \end{aligned}\tag{25}$$

where $A \approx 5\cdot 10^{-21}$ J is the Hamaker constant for PMMA-PHSA in n-dodecane,[17] r is the particle radius and $L = r + 10$ nm is half the interparticle separation (10 nm being the approximate thickness of the PHSA-layer[18]).

Another option is entanglement of the PHSA polymer chains that stabilize the PMMA particles,[4,17]

$$\begin{aligned} \Delta W_{\mathrm{ent}} &\sim & k_{\mathrm{B}}T_0\left(\tfrac{4\pi C^2}{3V_1\rho^2}\right)\left(\psi - \chi\right)\left(\delta - (h/2)\right)^2\\ && \cdot\left(3r + 2\delta + (h/2)\right)\\ &\approx & 10^3\ k_{\mathrm{B}}T_0\\ &\ll & 10^7\ k_{\mathrm{B}}T_0\ , \end{aligned}\tag{26}$$

in which ρ is the density of grafted chains, δ is the thickness of the PHSA-stabilizer shell, h is the surface-to-surface separation, C is the average concentration of polymer in the steric layer, $\psi(\chi)$ is an entropy (enthalpy) interaction parameter and V_1 is the partial molar volume of the solvent.

Instead of dilating, particle-laden liquid-liquid interfaces can bend when two droplets collide. The associated interparticle interaction can be ex-

pressed as[19]

$$
\begin{aligned}
\Delta W_{\mathrm{bend}} \quad &\sim \quad \left(\frac{\Delta W_{\mathrm{bending\ upon\ collision}}}{2}\right)\left(\frac{12}{n_{\mathrm{ip}}}\right) \\
&\approx \quad 6\left(\frac{r^2}{4\phi_{\mathrm{2D}}R^2}\right)(4\pi\gamma rR\cos(\theta)) \\
&\approx \quad 10^6\ k_{\mathrm{B}}T_0 \\
&\lesssim \quad 10^7\ k_{\mathrm{B}}T_0\ ,
\end{aligned}
\tag{27}
$$

with n_{ip} the (constant) number of interfacial particles, ϕ_{2D} the packing fraction of interfacial particles, R the droplet radius, γ the water-oil interfacial tension and θ the particle contact angle; we have assumed that each droplet has 12 neighbors (as in an fcc crystal). Note that, at high Φ, bending becomes less expensive than dilation,[19] which is why we observe in confocal microscopy that the particle-laden droplet surfaces bend rather than dilate at high Φ (or the Plateau borders would have filled up completely).

Finally, as centrifugation effectively increases the particle weight, we have considered flotation capillary forces. Following Ref.[20] we write

$$
\begin{aligned}
\Delta W_{\mathrm{flot}} \quad &\sim \quad 2\pi\gamma Q^2\ln\left(\frac{\gamma_{\mathrm{e}}qL}{2}\right) \\
&\sim \quad 10^{-1}\ k_{\mathrm{B}}T_0 \\
&\ll \quad 10^7\ k_{\mathrm{B}}T_0\ ,
\end{aligned}
\tag{28}
$$

in which

$$
Q \quad = \quad \tfrac{1}{6}q^2r^3\left(2 - 4D + 3\cos(\theta) - (\cos\theta)^3\right)\ ,
\tag{29}
$$

$$
q^2 \quad = \quad \frac{(\rho_{\mathrm{water}} - \rho_{\mathrm{oil}})\omega^2 d_{\mathrm{c}}}{\gamma}
\tag{30}
$$

and

$$
D \quad = \quad \frac{\rho_{\mathrm{solid}} - \rho_{\mathrm{oil}}}{\rho_{\mathrm{water}} - \rho_{\mathrm{oil}}}\ ,
\tag{31}
$$

with $\gamma_{\mathrm{e}} \approx 1.781$, ω the angular frequency and d_{c} the length of the centrifuge lever arm.

11 Movies
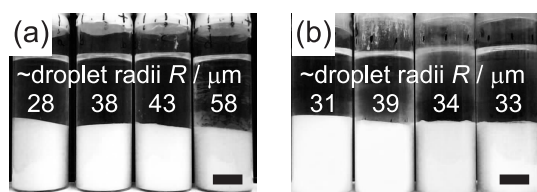

Figure 9: (a) *Movie3a_x1769rt.avi*. Recovery of water-in-dodecane emulsions, stabilized by 0.630 μm radius PMMA-PHSA particles, after centrifugation at $\sim$ 194g. (b) *Movie3c_x1516rt.avi*. Recovery of similar emulsions, from left to right stabilized by PMMA139-PLMA, PMMA110, PMMA063-PDV or PMMA058 (see Table 2), after centrifugation at $\sim$ 750g. Scale bars 10 mm; both movies have been JPEG compressed; spanning 24 h at (a) $\sim$ 1769$\times$ and (b) $\sim$ 1516$\times$ real-time.
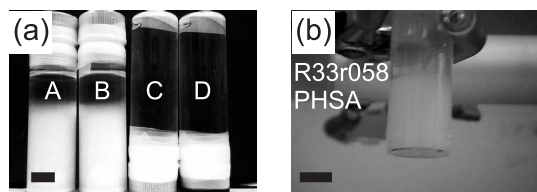

Figure 10: (a) *PMMA043_Movie_x1200rt.avi*. (A/B) 2.5 vol-% suspensions in n-dodecane of 0.425 μm radius PMMA-PHSA particles, after $\sim$ 41 h of gravitational sedimentation. (C/D) Similar samples, topped up with n-dodecane, 8 min after $\sim$ 15 h of centrifugation at $\sim$ 696g. Scale bar 10 mm; movie JPEG compressed; spanning $\sim$ 19 h at $\sim$ 1200$\times$ real-time. (b) *PMMA063_Shaker.avi*. Sample R33r058-PHSA, i.e. water-in-dodecane emulsion with mean droplet radius 33 μm and PMMA particle radius 0.575 μm, approximately two months after the expansion experiment corresponding to Fig. 7 – hardly any droplet/cell re-dispersion after $\sim$ 2.5 minutes on a flask shaker.

References

[1] M. Kogan, C. J. Dibble, R. E. Rogers and M. J. Solomon, Viscous solvent colloidal system for direct visualization of suspension structure, dynamics and rheology, *J. Colloid Interf. Sci.*, 2008, **318**, 252–263.

[2] *Dispersion Polymerization in Organic Media*, ed. K. E. J. Barrett, John Wiley & Sons, 1975.

[3] *Lange's Handbook of Chemistry*, ed. J. A. Dean, McGraw Hill Inc., 1999.

[4] S. Arditty, V. Schmitt, F. Lequeux and F. Leal-Calderon, Interfacial properties in solid-stabilized emulsions, *Eur. Phys. J. B*, 2005, **44**, 381–393.

[5] W. Rasband, *ImageJ*, http://rsb.info.nih.gov/ij, 2009.

[6] R. M. Wiley, Limited coalescence of oil droplets in coarse oil-in-water emulsions, *J. Coll. Sci.*, 1954, **9**, 427–437.

[7] H. M. Princen, Osmotic-Pressure of Foams and Highly Concentrated Emulsions .1. Theoretical Considerations, *Langmuir*, 1986, **2**, 519–524.

[8] S. Tcholakova, N. D. Denkov, I. B. Ivanov and B. Campbell, Coalescence in beta-lactoglobulin-stabilized emulsions: Effects of protein adsorption and drop size, *Langmuir*, 2002, **18**, 8960–8971.

[9] G. L. Squires, *Practical Physics*, Cambridge University Press, 1997.

[10] Re-emulsification: (5×30) s of vortex mixing with 2.5 min of rest in between cycles. Even though we did not initially observe any difference in behaviour between new and regenerated emulsions, we did notice that emulsions with $R > 50$ μm developed a macroscopic water phase at the bottom of the vial after about 10 re-emulsifications.

[11] S. Tcholakova, N. D. Denkov, I. B. Ivanov and B. Campbell, Coalescence stability of emulsions containing globular milk proteins, *Adv. Colloid Interfac.*, 2006, **123**, 259–293.

[12] We have noticed small differences in area fractions α determined using ImageJ and IDL, which we attribute to differences in RGB color to grayscale conversion.

[13] Note that we average over 8 positions, because the tops of the sediments are sometimes slanted, which we attribute to structural inhomogeneities in the samples rather than to problems with the centrifugation – the tops of sediments formed by centrifuging dispersions of PMMA in n-hexane are not slanted.

[14] T. G. Mason, M. D. Lacasse, G. S. Grest, D. Levine, J. Bibette and D. A. Weitz, Osmotic pressure and viscoelastic shear moduli of concentrated emulsions, *Phys. Rev. E*, 1997, **56**, 3150–3166.

[15] V. G. Babak and M. J. Stebe, Highly concentrated emulsions: Physicochemical principles of formulation, *J. Disper. Sci. Technol.*, 2002, **23**, 1–22.

[16] P. A. Kralchevsky, V. N. Paunov, I. B. Ivanov and K. Nagayama, Capillary Meniscus Interaction between Colloidal Particles Attached to a Liquid-Fluid Interface, *J. Colloid Interf. Sci.*, 1992, **151**, 79–94.

[17] R. J. R. Cairns, W. van Megen and R. H. Ottewill, A Comparison between Theoretically Computed and Experimentally Measured Pressures for Interacting Sterically Stabilized Particles, *J. Colloid Interf. Sci.*, 1981, **79**, 511–517.

[18] R. J. R. Cairns, R. H. Ottewill, D. W. J. Osmond and I. Wagstaff, Studies on Preparation and Properties of Lattices in Nonpolar Media, *J. Colloid Interf. Sci.*, 1976, **54**, 45–51.

[19] P. A. Kralchevsky, I. B. Ivanov, K. P. Ananthapadmanabhan and A. Lips, On the thermodynamics of particle-stabilized emulsions: Curvature effects and catastrophic phase inversion, *Langmuir*, 2005, **21**, 50–63.

[20] V. N. Paunov, P. A. Kralchevsky, N. D. Denkov and K. Nagayama, Lateral Capillary Forces between Floating Submillimeter Particles, *J. Colloid Interf. Sci.*, 1993, **157**, 100–112.